

Dynamic Guidance Virtual Fixtures for Guiding Robotic Interventions: Intraoperative MRI-guided Transapical Cardiac Intervention Paradigm

Jhasketan Padhan
Department of Surgery
Hamad Medical Corporation
Doha, Qatar

Julien Abinahed
Department of Surgery
Hamad Medical Corporation
Doha, Qatar
jabinahed@hamad.qa

Nikolaos Tsekos
Department of Computer Science
University of Houston
Houston, Texas

Zhigang Deng
Department of Computer Science
University of Houston
Houston, Texas
zdeng4@central.uh.edu

Abdulla Al-Ansari
Department of Surgery
Hamad Medical Corporation
Doha, Qatar

Nikhil V. Navkar
Department of Surgery
Hamad Medical Corporation
Doha, Qatar
nnavkar@hamad.qa

Abstract—The advent of intraoperative real-time image guidance has led to the emergence of new surgical interventional paradigms including image-guided robot assistance. Most often the use of an intraoperative imaging modality is limited to visual perception of the area of procedure. In this work, we propose a system for performing interventions with real-time Magnetic Resonance Imaging (rtMRI). The described computational core, processes on-the-fly rtMRI and generates dynamic guidance virtual fixture that in turn is used to update visualization and a force-feedback interface. The system was experimentally tested by applying it to a simulated Transapical Aortic Valve Implantation with a virtual robotic manipulator. The study results demonstrate significant improvement in the surgical task by decreasing the duration of the procedure and increasing safety in the presence of cardiac and breathing motion.

Keywords—MR guided interventions, real time MRI, MR compatible robots, virtual fixture, robot-assisted interventions

I. INTRODUCTION

The potential of real-time imaging to track tissue motion and use it for the safe and accurate maneuvering of interventional tools inside the dynamic environment of the patient's body may lead to new minimally invasive surgical or interventional paradigms. Within this context, pioneering works have led to the introduction and investigation of Virtual Fixture (VF), i.e., virtual overlays that describe spatio-temporal constraints for safe and accurate maneuvering of an interventional tool inside the patient's body [1]–[4]. The potential of VF to guide a procedure has been investigated on paradigms of cardiac surgeries (e.g., coronary artery bypass graft [2], pulmonary vein isolation [1], and aortic valve deployment [3]). Those studies clearly demonstrate the power of VF to guide a tool along the surface of the beating heart. Among various categories of VFs, Dynamic Guidance Virtual Fixtures (DGVF) [4] assists the operator to move an interventional tool along a desired dynamic path

towards the targeted tissue through a continuously changing environment. Such DGVF, if generated on-the-fly from the imaging information of the area of the procedure (AoP), can be highly beneficial for minimally-invasive, image-guided procedures including intracardiac ones, such as valvuloplasties [5], mitral-valve clip repair, or ablations on the beating heart [6], [7]. In addition, they can also be used for guiding interventions at other sites, such as prostate [8]–[10] and breast [11], [12].

In prior works, VFs for cardiac interventions are generated based on pre-operative images, and then co-registered and superimposed to real-time intraoperative Ultrasound (US) images [4]. To address the low image quality of US, intraoperative US images are registered on-the-fly with pre-operative dynamic high resolution and contrast images such as breath-hold cinematic MRI [4] or CT [1], [2]. Such intra-operative registration may not be robust enough to account for unpredictable, substantial, and transient or sustained deformations of tissue secondary to the procedure or natural motion (e.g. irregular heart beat and breathing) [4]. In principle, such a mismatch can be obviated when the same modality is used during the surgical procedure to collect high-resolution real-time data and generate the VFs. Recent advances, such as the reduction of acquisition times in real-time MRI [13] and MR-compatible robotics [14], [15], offer the opportunity to perform procedures with intraoperative MR guidance. This addresses the challenge associated with the aforementioned multi-modality co-registration and can lead to new opportunities in using DGVF. The technique of generating virtual fixtures from real-time MRI for cardiac intervention was previously presented by Navkar et al. [3], [16]. A dynamic virtual 3D corridor was generated from tissue boundaries of left ventricle extracted from rtMRI. It was an example of a forbidden region virtual fixture, where forces were exerted on the interface controlling the robotic

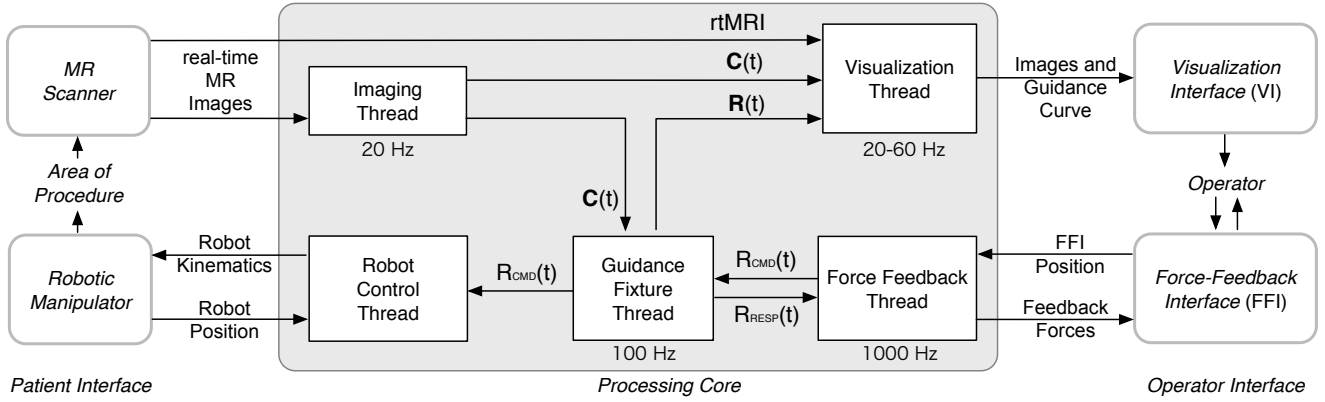


Figure 1. System architecture illustrating interconnection of the modules of the processing core, the operator interface (comprising of force feedback interface and visualization interface) and sensing at the area of procedure via the patient interface (comprising of robotic manipulator and MR scanner).

manipulator if it goes close to the tissue boundary. Similarly in [16], a tip of a straight intervention tool was controlled along a path. As compared to previous work, this work presents the concept of guiding an entire body of a bendable manipulator along a dynamic curve via generation of DGVF.

The goal of this work is the development of a system for on-the-fly generation of DGVF from real-time MRI, and its use to update a visual interface (VI) and drive a force-feedback interface (FFI) for human-in-the-loop control of a generic actuated manipulator. To the best of our knowledge, this is the first reported effort to demonstrate the use of intraoperative real-time imaging for the on-the-fly generation of DGVF. The proposed system was tested considering the clinical paradigm of Transapical Aortic Valve Implantation (TA-AVI), which is under investigation by several groups [17]–[20]. This procedure was particularly selected as an appropriate test bed for on-the-fly extraction of DGVF, since it entails traversing the dynamic environment of Left Ventricle (LV), from the apical entrance to the moving aortic root for the deployment of a prosthetic valve.

II. METHODOLOGY

Figure 1 shows the architecture of the proposed telemanipulation system delineating its three components and the flow of data and information among them: (i) the system-to-patient interface, i.e., the MR scanner and a generic robotic manipulator, (ii) the system-to-operator interface, i.e., the aforementioned VI and FFI, and (iii) the processing core composed of task-specific parallel running threads. In brief, the imaging thread processes rtMRI data on-the-fly, received from the MR scanner via a TCP/IP connection, and generates a dynamic guidance curve $\mathbf{C}(t)$ (§II-A), i.e., the path that must be followed for safe maneuvering into the AoP. The $\mathbf{C}(t)$ is then used by the visualization and the guidance fixture threads. The former updates the VI. The latter performs two tasks (§II-B): (i) computing the position $\mathbf{R}(t)$ of the virtual manipulator and (ii) generating

the DGVF that provides *expert-advisory* to the operator in the form of feedback forces via the FFI. Via the VI and FFI, the DGVF is used to guide the operator to follow the $\mathbf{C}(t)$. Corresponding to the robot-maneuvering command $R_{CMD}(t)$ (entered from the FFI via the force-feedback thread), an appropriate response $R_{RESP}(t)$ is generated and sent back to the force-feedback thread. The force-feedback thread computes and renders the feedback forces on the FFI to constrain the motion of a robotic manipulator along the curve $\mathbf{C}(t)$. The visualization thread renders the dynamic guidance curve $\mathbf{C}(t)$ and the position $\mathbf{R}(t)$ of the virtual manipulator and then superimposes them onto corresponding real-time MR images on the VI. The robot control thread would be used to control the robotic manipulator inside the MR scanner, and its design is beyond the scope of this work.

A. Generation of Guidance Curves

Currently, rtMRI of the beating heart with acceptable quality for interventions can be collected with a speed in the range of 30-50 ms/slice [13]. Therefore, to track anatomical landmarks pertinent to the procedure (that cannot be imaged with a single plane), we adopt a method that collects a small number of slices and processes them on-the-fly using a pipeline proposed previously by Navkar et al. [19]. This pipeline collects non-triggered, oblique-to-each-other slices ($I_k(t); k = 1, 2, 3$) in an interleaved fashion and extracts the *boundary points* $\mathbf{P}_{i,j}(t)$ that track the endocardium and the aortic root (Fig. 2a). Note that the coordinates of the boundary points $\mathbf{P}_{i,j}(t) \in \mathbb{R}^3$ are measured relative to the inherent coordinate system of the MR scanner.

The boundary points $\mathbf{P}_{i,j}(t)$ are then interconnected with splines (Fig. 2b) to generate the control curves $\mathbf{C}_i(t)$ ($i = 1$ to 4), where $\mathbf{C}_1(t)$ and $\mathbf{C}_3(t)$ are on slice $I_1(t)$, and $\mathbf{C}_2(t)$ and $\mathbf{C}_4(t)$ are on slices $I_2(t)$ to $I_3(t)$. From those data, the boundary of the endocardium is generated by linear interpolation between points $\mathbf{P}_{i,1}(t)$ and $\mathbf{P}_{i,2}(t)$ ($i = 1$ to 4). The tissue-to-blood boundary inside the aortic root is generated

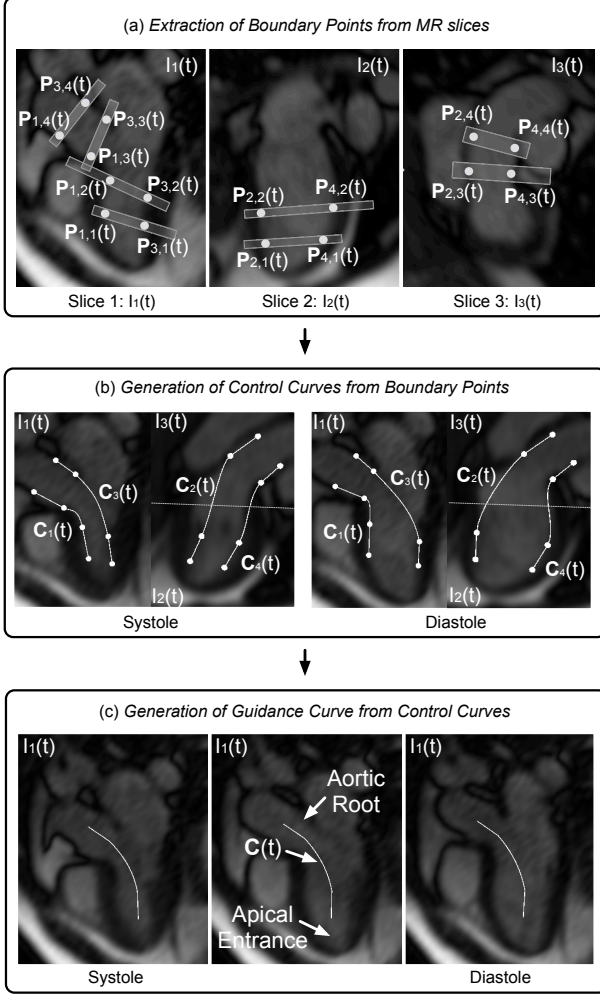


Figure 2. Generation of the guidance curve $C(t)$ from real-time interleaved multislice MR images.

by linear interpolation between the boundary points $P_{i,3}(t)$ and $P_{i,4}(t)$ on slices $I_1(t)$ and $I_3(t)$. The region between the point $P_{i,2}(t)$ and $P_{i,3}(t)$ is interpolated using Kochanek-Bartels curves [21]. If needed, the tangential properties of the control curves can be altered by the operator manually (to adjust their deflection from the apex to the aorta); as an example, depending on the specific patient's anatomy, the curves can be deflected more towards the interventricular septum compared to the mitral valve and papillary muscles or vice versa. The control curves are generated such that the number of interpolated points remains the same on all the curves and all the time frames. The resultant guidance curve $C(t)$ is then computed as the average of the four control curves (i.e., $C(t) = \sum_{i=1}^4 C_i(t)/4$), as shown in Fig. 2c.

In our system, the imaging thread requires 0.20 ms for the computation of the dynamic guidance curve from rtMRI, as in [19]. However, since each slice is collected every 50 ms (which is the actual bottleneck of the pipeline) the effective frequency of the thread is assigned to be same as the rtMRI, i.e. 20 Hz.

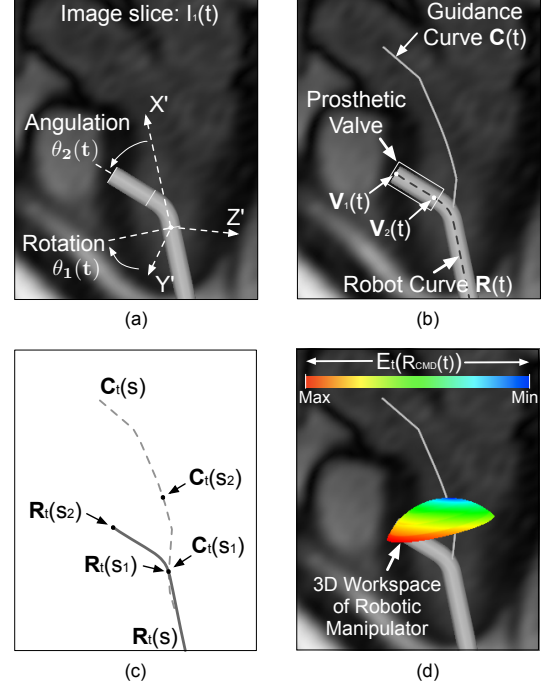


Figure 3. (a) The two DoFs (rotation and angulation) of the virtual robotic manipulator measured in the distal $X'Y'Z'$ coordinate frame. (b) Definitions of the curve $R(t)$ that represents the robot, guidance curve $C(t)$ and the end points $V_1(t)$ and $V_2(t)$ of the prosthetic valve (c) Parameterized representation of the curves. (d) Workspace of the robotic manipulator color-coded as per the alignment energy function.

B. Generation of Dynamic Guidance Virtual Fixtures

The DGVF is generated by using the maneuvering command $R_{CMD}(t)$, the guidance curve $C(t)$, and the predefined kinematics f_k of a generic robotic manipulator. As in most of commercial catheter systems, our implementation of the virtual tubular manipulator exhibits two Degree of Freedoms (DoFs), i.e., angulation and rotation. In our studies, both the rotation (θ_1) and angulation (θ_2) angles are measured with respect to the distal coordinate system (Fig. 3a), which is positioned by using a tracking algorithm [19], [22]. The robot structure is described with a curve $R(t)$ along the center axis of the manipulator (Fig. 3b) measured relative to the MR scanner coordinate. An example of a similar robotic manipulator structure is presented in Velasquez et al. [23] and Yeniaras et al. [24]. The position $R(t)$ is computed by the guidance thread from the input maneuvering command $R_{CMD}(t)$, such that $R(t) = f_k(R_{CMD}(t))$, where f_k is the composite transformation that describes the forward kinematics and its specific form depends on the design and kinematic structure of the robotic manipulator. The input maneuvering command is described with an array $R_{CMD}(t) = (\theta_i(t); i = 1 \text{ to } M)$, where $\theta_i(t)$ is the degree of actuation of the i^{th} actuator of the robot. We further represent all possible commands that can be issued by operator as R_{SET} .

The purpose of the DGVF is to direct the posture of the manipulator to comply with the guidance curve,

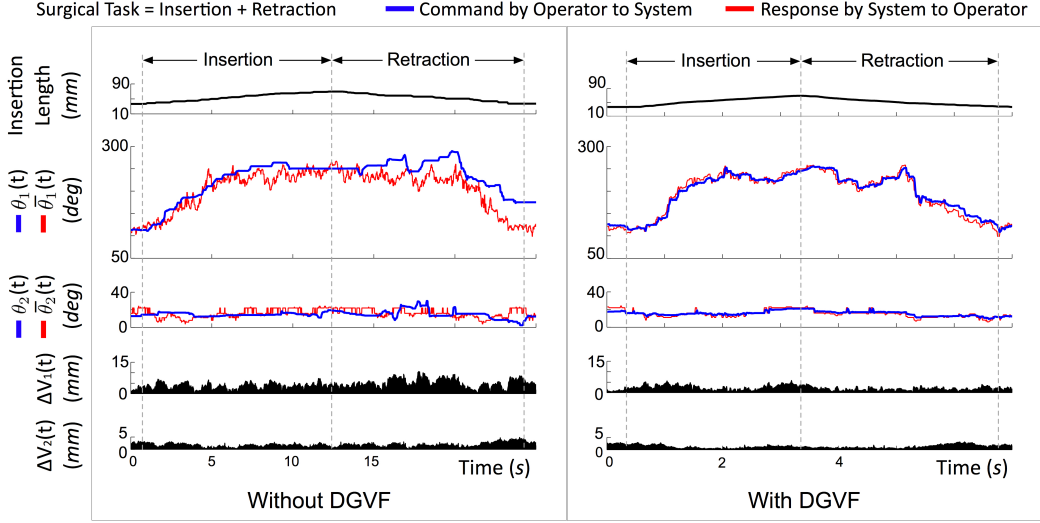


Figure 4. Representative results from one subject that performed the task of maneuvering the virtual prosthetic valve in the (a) absence and (b) presence of DGVs.

i.e. the curve $\mathbf{R}(t)$ (representing the robot) to match the dynamic guidance curve $\mathbf{C}(t)$ for a time instance t . To computationally perform this operation, both the curves are parameterized by the arc length s in an open interval $I = (s_1, s_2)$, i.e. $\mathbf{R}_t : I \rightarrow \mathbb{R}^3$ and $\mathbf{C}_t : I \rightarrow \mathbb{R}^3$. An alignment energy function E_t is then computed starting from $s = s_1$ to $s = s_2$ (shown in Fig. 3c):

$$E_t(R_{CMD}(t)) = \int_{s_1}^{s_2} w(s) \|\mathbf{R}_t(s) - \mathbf{C}_t(s)\| ds. \quad (1)$$

Here $w(s)$ is a weighting function along the robotic manipulator length and is adjusted manually by the operator. It allows the operator to give preference to different components of the robotic manipulator for alignment with $\mathbf{C}_t(s)$.

A response command is generated at time t by finding a suitable command $R_{RESP}(t) \in R_{SET}$, for which E_t is minimum using gradient descent optimization. The response is represented by an array $R_{RESP}(t) = (\bar{\theta}_i(t); i = 1 \text{ to } M)$, where $\bar{\theta}_i(t)$ is the degree of actuation of the i^{th} actuator of the FFI. The function $w(s)$ is set manually such that $E_t(R_{CMD}(t))$ has one minima. Figure 3d shows E_t color-coded for the workspace of the robotic manipulator. E_t is minimum near the vicinity of the curve and increases as the tool moves away from curve towards the tissue. The guidance fixture thread requires at most 10 ms to compute $R_{RESP}(t)$ based on the input $R_{CMD}(t)$, thus allowing the thread to run at 100 Hz. The feedback forces/torques are computed by the force feedback thread for the i^{th} actuator of FFI by implementing a virtual spring damper between current angle, $\theta_i(t)$, and the one desired by the system, $\bar{\theta}_i(t)$.

C. Hardware

The imaging, visualization, and guidance fixture threads of the processing core (Fig. 1) were implemented on a

dedicated PC (Intel 3.2GHz; 12GB RAM). The force-feedback thread was running on an embedded controller board (DS1103 PPC, dSPACE) that provided I/O, A/D, and D/A interfacing and was connected to the PC via a 100 Mbps optical cable. A two DoFs FFI was used for one-to-one mapping between the operator input $R_{CMD}(t)$ (i.e. angles $\theta_1(t)$ and $\theta_2(t)$) by means of two DC motors (Maxon 264571) with their encoders and amplifiers connected to the controller board. To adjust insertion and retraction of the virtual tool we used a pedal controller (Logitech Flight System G940) connected to the dedicated PC (passive without force-feedback).

III. EXPERIMENTAL STUDIES

To address logistics with the availability of the MR scanner, experiments were performed off-line (i.e. the system was not connected to the scanner). Specifically, we used a virtual MR scanner that supplied the imaging thread with a stream of previously collected real-time MR images with the exact timing of their collection, i.e. every 50 ms, to mimic on-line conditions. The data included I_1 , I_2 , and I_3 multislice sets each of 540 rtMRI images (non-triggered free-breathing, pixel size: $1.25 \times 1.25 \text{ mm}^2$, FOV: $275 \times 400 \text{ mm}^2$, slice thickness: 6 mm, TR: 49.3 ms, TE: 1 ms) collected on a Siemens 1.5T Avanto MR scanner on healthy volunteers. The stream was repeated as long as needed to perform the task.

The performance of the introduced DGVF was investigated by maneuvering a virtual robotic manipulator for the hypothetical clinical scenario of a TA-AVI [17]–[19]. This manipulator is 8-mm wide tubular structure which is inserted inside LV, and its distal-end is endowed with two DoFs controlled by the FFI: one for rotation $\theta_1(t)$ and the other for angulation $\theta_2(t)$ (Fig. 3a). In addition, it is assumed that

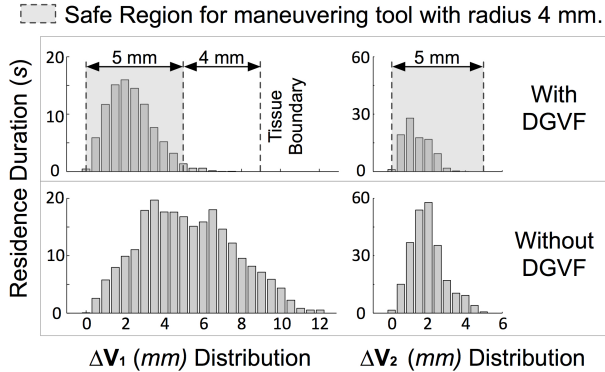


Figure 5. Histograms illustrating the distribution of distances ΔV_1 and ΔV_2 for all five subjects.

it carries a prosthetic valve located between points \mathbf{V}_1 and \mathbf{V}_2 (Fig. 3b). After initial training for acquaintance with the interfaces and development of hand-eye coordination, five subjects maneuvered the virtual manipulator from the apex to the aortic annulus simulating the delivery of the valve. This task was performed twice, one with and one without the DGVF. During the maneuvering, we continuously recorded the R_{CMD} , R_{RESP} , time-stamps and the shortest distances ΔV_1 and ΔV_2 of points \mathbf{V}_1 and \mathbf{V}_2 from the curve $\mathbf{C}(t)$.

IV. RESULTS

Figure 4 presents representative results from one subject that show the $\theta_1(t)$, $\theta_2(t)$, ΔV_1 and ΔV_2 during the task. As compared to the case without the DGVF, with the DGVF the angles $\theta_1(t)$ and $\theta_2(t)$ commanded by the operator more closely follow $\bar{\theta}_1(t)$ and $\bar{\theta}_2(t)$ generated by the system (Fig. 4). As a consequence, the distances of the valve end-points ΔV_1 and ΔV_2 from the $\mathbf{C}(t)$ were reduced when the DGVF was used from 4.1 ± 1.9 mm to 2.0 ± 1.1 mm and 1.8 ± 0.9 mm to 1.3 ± 0.7 mm, respectively, for ΔV_1 and ΔV_2 . Those data show that force-feedback assisted the subjects to follow the desired angles $\theta_1(t)$ and $\theta_2(t)$ with a higher accuracy due to compliance to the guidance curve $\mathbf{C}(t)$, as well as safer maneuvering (i.e., sufficiently away from the endocardium). It is also noteworthy that for the particular subject in Fig. 4, with the DGVF, the task required 6.8 s while the case without the DGVFs required 24 s.

Figure 5 shows the total time spent by all the five subjects for different distribution of distances ΔV_1 and ΔV_2 , i.e. residence time of the end-points of the valve at a given distance from $\mathbf{C}(t)$. Those histograms offer another appreciation of the compliance of maneuvering to $\mathbf{C}(t)$, with and without the DGVF. It is evident that the distributions are far narrower for both ΔV_1 and ΔV_2 , demonstrating that with the DGVFs the operator maintained the virtual robot within a far narrower range. This is consistent with a higher accuracy, as well as safety. In addition, it provides us with an appreciation of the available space: assuming that in end-systole the shortest distance of the $\mathbf{C}(t)$ to the endocardium is 9 mm measured inside LV, a tool with 4 mm radius stays

in a *safe region* (shaded in Fig. 5) for 98% of the task time; i.e., the points \mathbf{V}_1 and \mathbf{V}_2 stay within a distance of 5 mm from $\mathbf{C}(t)$. The surgical task time also decreased from 24.21 ± 4.41 s to 9.41 ± 4.37 s.

V. DISCUSSION

The proposed system describes an approach for generating on-the-fly DGVF from rtMRI that improves the accuracy of maneuvering, while ensuring safety, decreases the overall duration of the procedure (i.e., by 2.5 times), and maintains the tool within a well-defined conduit. The proposed method can be used in other interventional paradigms, as example control curves (§II-A) can be generated outside the heart surface for pericardial procedures. Parallel processing can also be used for calculating the R_{RESP} (§II-B) for more complex robotic structures.

The presented work has certain limitations. First, the study was performed off-line in a virtual environment. No MR scanner was connected to the system. To overcome this limitation and to ensure realism and accurate timing, previously collected real-time MR images feeds were used and fed to the system for generating DGVF. The robotic manipulator was simulated in a virtual environment and need to address actuation delays and response time in the future work. However, this does not affect the way the fixtures are computed from the image data. In the future, we plan to focus on the incorporation of a realistic virtual robot and methods to address actuation delays and their effect on the stability of the system [24], [25]. Second, we plan to explore DVGF with mixed reality environments where holograms of the anatomical structures enhances the perception of the intervention site [26], [27].

VI. CONCLUSION

Concluding this work, DGVF generated from intraoperative imaging modality hold potentials for better navigation of intervention tools in image-guided robot assisted interventions, thus reducing the duration of the procedure and improving the safety.

ACKNOWLEDGMENT

This work was supported by National Priority Research Program (NPRP) award (NPRP13S-0116-200084) from the Qatar National Research Fund (a member of The Qatar Foundation) and IRGC-04-JI-17-138 award from Medical Research Center (MRC) at Hamad Medical Corporation (HMC). All opinions, findings, conclusions or recommendations expressed in this work are those of the authors and do not necessarily reflect the views of our sponsors.

REFERENCES

- [1] K. Kwok, G. Mylonas, L. Sun, M. Lerotic, J. Clark, T. Athanasiou *et al.*, "Dynamic active constraints for hyper-redundant flexible robots." in *Medical Image Computing and Computer Assisted Intervention*, 2009, pp. 410 – 417.

- [2] S. Park, R. D. Howe, and D. F. Torchiana, "Virtual fixture for robotic cardiac surgery," in *Medical Image Computing and Computer Assisted Intervention*, 2001, pp. 1419 – 1420.
- [3] N. V. Navkar, Z. Deng, D. J. Shah, and N. V. Tsekos, "A framework for integrating real-time mri with robot control: Application to simulated transapical cardiac interventions," *IEEE Transactions on Biomedical Engineering*, vol. 60, no. 4, pp. 1023–1033, 2013.
- [4] J. Ren, R. Patel, K. McIsaac, G. Guiraudon, and T. Peters, "Dynamic 3-d virtual fixtures for minimally invasive beating heart procedures," *IEEE Transaction on Medical Imaging*, vol. 27, no. 8, pp. 1061–1070, 2008.
- [5] J. L. Chan, D. Mazilu, J. G. Miller, T. Hunt, K. A. Horvath, and M. Li, "Robotic-assisted real-time MRI-guided TAVR: from system deployment to in vivo experiment in swine model," *Int J Comput Assist Radiol Surg*, vol. 11, no. 10, pp. 1905–1918, Oct 2016.
- [6] K.-H. Lee, K. C. D. Fu, Z. Guo, Z. Dong, M. C. W. Leong, C.-L. Cheung, A. P.-W. Lee, W. Luk, and K.-W. Kwok, "Mr safe robotic manipulator for mri-guided intracardiac catheterization," *IEEE/ASME Transactions on Mechatronics*, vol. 23, no. 2, pp. 586–595, 2018.
- [7] Z. Dong, X. Wang, G. Fang, Z. He, J. D.-L. Ho, C.-L. Cheung, W. L. Tang *et al.*, "Shape tracking and feedback control of cardiac catheter using mri-guided robotic platform—validation with pulmonary vein isolation simulator in mri," *IEEE Transactions on Robotics*, pp. 1–18, 2022.
- [8] J. D. Velazco-Garcia, N. V. Navkar, S. Balakrishnan, J. Abin角度, A. Al-Ansari, A. Darweesh, Al-Rumaihi *et al.*, "Evaluation of interventional planning software features for mr-guided transrectal prostate biopsies," in *2020 IEEE 20th International Conference on Bioinformatics and Bioengineering (BIBE)*, 2020, pp. 951–954.
- [9] J. D. Velazco-Garcia, N. V. Navkar, S. Balakrishnan, J. Abin角度, A. Al-Ansari *et al.*, "Preliminary evaluation of robotic transrectal biopsy system on an interventional planning software," in *2019 IEEE 19th International Conference on Bioinformatics and Bioengineering (BIBE)*, 2019, pp. 357–362.
- [10] J. D. Velazco-Garcia, N. V. Navkar, S. Balakrishnan, J. Abin角度, K. Al-Rumaihi, A. Darweesh *et al.*, "End-user evaluation of software-generated intervention planning environment for transrectal magnetic resonance-guided prostate biopsies," *Int J Med Robot*, vol. 17, no. 1, pp. 1–12, Feb 2021.
- [11] P. Gao, X. Kong, Y. Song, Y. Song, Y. Fang *et al.*, "Recent Progress for the Techniques of MRI-Guided Breast Interventions and their applications on Surgical Strategy," *J Cancer*, vol. 11, no. 16, pp. 4671–4682, 2020.
- [12] R. Monfaredi, K. Cleary, and K. Sharma, "MRI Robots for Needle-Based Interventions: Systems and Technology," *Ann Biomed Eng*, vol. 46, no. 10, pp. 1479–1497, Oct 2018.
- [13] M. Guttman, C. Ozturk, A. Raval, V. Raman, A. Dick, R. DeSilva *et al.*, "Interventional cardiovascular procedures guided by real-time mr imaging: an interactive interface using multiple slices, adaptive projection modes and live 3d renderings," *Journal of Magnetic Resonance Imaging*, vol. 26, no. 6, pp. 1429–1435, 2007.
- [14] N. Tsekos, A. Khanicheh, E. Christoforou, and C. Mavroidis, "Magnetic resonance - compatible robotic and mechatronics systems for image-guided interventions and rehabilitation: A review study," *Annual Review of Biomedical Engineering*, vol. 9, pp. 351 – 387, 2007.
- [15] E. Yeniaras, N. Navkar, M. A. Syed, and N. V. Tsekos, "A computational system for performing robot-assisted cardiac surgeries with mri guidance," in *2010 Society for Design and Process Science (SDPS)*, 2010.
- [16] N. V. Navkar, Z. Deng, D. J. Shah, K. E. Bekris, and N. V. Tsekos, "Visual and force-feedback guidance for robot-assisted interventions in the beating heart with real-time mri," in *2012 IEEE International Conference on Robotics and Automation*, 2012, pp. 689–694.
- [17] K. Horvath, D. Mazilu, O. Kocaturk, and M. Li, "Transapical aortic valve replacement under real-time magnetic resonance imaging guidance: experimental results with balloon-expandable and self-expanding stents," *European Journal of Cardio-thoracic Surgery*, vol. 39, no. 6, pp. 822–828, 2010.
- [18] M. Li, A. Kapoor, D. Mazilu, and K. Horvath, "Pneumatic actuated robotic assistant system for aortic valve replacement under mri guidance," *IEEE Transaction on Biomedical Engineering*, vol. 58, no. 2, pp. 443 – 451, 2011.
- [19] N. Navkar, E. Yeniaras, D. Shah, N. Tsekos, and Z. Deng, "Generation of 4d access corridors from real-time multislice mri for guiding transapical aortic valvuloplasties," in *Medical Image Computing and Computer Assisted Intervention*, 2011, pp. 249 – 257.
- [20] E. Yeniaras, N. V. Navkar, A. E. Sonmez, D. J. Shah, Z. Deng, and N. V. Tsekos, "MR-based real time path planning for cardiac operations with transapical access," *Med Image Comput Assist Interv*, vol. 14, no. Pt 1, pp. 25–32, 2011.
- [21] D. Kochanek and R. Bartels, "Interpolating splines with local tension, continuity, and bias control," *SIGGRAPH Computer Graphics*, vol. 18, no. 3, pp. 33 – 41, 1984.
- [22] X. Gao, N. V. Navkar, D. J. Shah, N. V. Tsekos, and Z. Deng, "Intraoperative registration of preoperative 4d cardiac anatomy with real-time mr images," in *2012 IEEE 12th International Conference on Bioinformatics Bioengineering (BIBE)*, 2012, pp. 583–588.
- [23] C. A. Velasquez, N. V. Navkar, A. Alsaied, S. Balakrishnan, J. Abin角度, A. A. Al-Ansari *et al.*, "Preliminary design of an actuated imaging probe for generation of additional visual cues in a robotic surgery," *Surg Endosc*, vol. 30, no. 6, pp. 2641–2648, 06 2016.
- [24] E. Yeniaras, J. Lamaury, N. V. Navkar, D. J. Shah, K. Chin, Z. Deng *et al.*, "Magnetic resonance based control of a robotic manipulator for interventions in the beating heart," in *2011 IEEE International Conference on Robotics and Automation*, 2011, pp. 6270–6275.
- [25] J. D. Velazco Garcia, N. V. Navkar, D. Gui, C. M. Morales, E. G. Christoforou, A. Ozcan *et al.*, "A Platform Integrating Acquisition, Reconstruction, Visualization, and Manipulator Control Modules for MRI-Guided Interventions," *J Digit Imaging*, vol. 32, no. 3, pp. 420–432, 06 2019.
- [26] J. D. Velazco-Garcia, N. V. Navkar, S. Balakrishnan, G. Younes, J. Abin角度, K. Al-Rumaihi *et al.*, "Evaluation of how users interface with holographic augmented reality surgical scenes: Interactive planning MR-Guided prostate biopsies," *Int J Med Robot*, vol. 17, no. 5, p. e2290, Oct 2021.
- [27] C. M. Morales Mojica, J. D. Velazco Garcia, N. V. Navkar, S. Balakrishnan, J. Abin角度, W. El Ansari *et al.*, "A Prototype Holographic Augmented Reality Interface for Image-Guided Prostate Cancer Interventions," in *Eurographics Workshop on Visual Computing for Biology and Medicine*, 2018.